Water Reuse

IWA PUBLISHING

Water Reuse Vol 14 No 1, 16 doi: 10.2166/wrd.2024.086

Seeded membrane distillation crystallization for hypersaline brine treatment

Stefanie Flatscher [a], Florian Hell[b], Mark W. Hlawitschka[a,*] and Josef Lahnsteiner [b]

[a] Institute of Process Engineering, Johannes Kepler University Linz, Altenberger Strasse 69, Linz 4040, Austria
[b] VA TECHWABAG GmbH, Dresdner Strasse 89-91, Vienna 1200, Austria
*Corresponding author. E-mail: mark.hlawitschka@jku.at

SF, 0009-0001-7991-3712

ABSTRACT

Brine evaporation and crystallization are energy- and equipment-intensive technologies commonly used in industries. Alternatively, membrane distillation (MD) has shown ability for concentrating different saline solutions. However, there is a limited understanding of the impact of these solutions on the scaling and wetting behavior. To address this knowledge gap and reduce costs and energy consumption, we investigated a novel method called 'seeded near-zero liquid discharge membrane crystallization' (NZLDMC). This approach combines MD and crystallization in a single apparatus, reducing capital and operating costs while improving sustainability. Our study focused on applying seeding processes at NZLDMC for concentrating synthetic mono- and multi-salt solutions with a salinity of 300 g/L and a real salt solution. We investigated the effects of salt crystals and seeds on membrane performance under different operating conditions. Our findings indicate that seeding crystal technology leads to high yield and long-term stability, thereby offering the potential in industries and municipal water treatment to fractionate salt in multi-salt solutions and obtain purified water simultaneously.

Key words: membrane crystallization, membrane distillation crystallization, near-zero liquid discharge, seeding technology

HIGHLIGHTS

- The seeded membrane distillation crystallization process allows the treatment of highly concentrated salt solutions.
- The absence of membrane scaling is a benefit of seed crystals for long-term stability.
- Using a membrane distillation and crystallization process in a single unit reduces capital and operating costs while improving sustainability.

INTRODUCTION

Severe water shortages affect over 4 billion people worldwide for at least 1 month each year, and the scarcity is driven by climate change and industrial expansion (Mekonnen & Hoekstra 2016; Dehghani *et al.* 2022). In particular, arid areas in Europe and America face persistent challenges in obtaining clean water, leading to economic and environmental consequences (Hristov *et al.* 2021). Desalination improves tap water supplies in arid regions and coastal cities (Al-Agha & Mortaja 2005; Shomar & Hawari 2017). Desalination and industrial processes generate considerable brine waste. The world produces more than 100 million m^3/d of water from desalination, leaving an even higher volume of concentrated brine (141.5 million m^3/d) (Jones *et al.* 2019). The disposal of brine poses a fundamental challenge. Common practices include direct disposals into the environment, such as surface water discharge, evaporation ponds, deep-well injection, and direct land applications, which can increase the salinity of surface water and harm the environment (Drioli *et al.* 2012; Creusen *et al.* 2013; Panagopoulos *et al.* 2019). The brine has thereby typical salinities of 70–85 g L^{-1}, resulting in large amounts of contaminated water that could be recovered.

Addressing these challenges, zero liquid discharge (ZLD) processes have emerged as effective approaches in recovering a large amount of water from the rejected brine, reducing environmental impact and promoting sustainability (Almasri *et al.* 2015). Wastewater-free production has become a focal point in recent decades, partly driven by concerns about regulatory fines associated with improper wastewater management (Raff & Earnhart 2018). The ZLD technology employs a closed resource and water cycle to prevent saltwater release into the environment, which requires the crystallization process (Panagopoulos 2021; Date *et al.* 2022). In the context of high salt content and brine waste, ZLD is integrated with

membrane-based water desalination processes (Conidi *et al.* 2018; Damtie *et al.* 2019; Zhao *et al.* 2020). Solar evaporation and wind-assisted intensified evaporation technology (WAIV) are commonly used methods for handling brine waste (Gilron *et al.* 2003; Bello *et al.* 2021). Solar evaporation consists of leaving the rejected water in a pond, where the water evaporates due to the sun. WAIV is an alternative to solar evaporation ponds and uses wind energy to evaporate the water (Ahmad & Baddour 2014; Morillo *et al.* 2014; Bello *et al.* 2021; Shah *et al.* 2022).

An innovative process to solve this problem is membrane distillation (MD) crystallization, which allows the recovery of water and raw materials from the brine solution. This process minimizes the brine volume considerably and results in a near-ZLD. MDC is a combination of MD and crystallization. MD represents an innovative membrane-based process that handles highly saline solutions, making it ideal for water production (Peters & Hankins 2021; Julian *et al.* 2022). MD is a separation process that utilizes hydrophobic membranes to allow water vapor molecules to pass due to the vapor pressure difference across the membrane (Rao *et al.* 2014; Gustafson *et al.* 2018). The main product of MD is water, while the remaining feed solution is highly concentrated. This creates a favorable situation for crystallizing the salts in the solution. Obtaining supersaturation allows crystals to be produced from the feed solution.

Previous studies have shown several challenges to overcome when developing a feasible MDC process for the treatment of high-saline solutions, such as unwanted crystallization in the membrane module and crystal blockages in the connecting tubes between the membrane module and the crystallizer (Tun *et al.* 2005; Guan *et al.* 2012). Therefore, the selection of the correct operating parameters is essential to avoid crystal deposits and enable the long-term operation of the process to obtain high water and salt recovery rates (Chen *et al.* 2014). For example, typical operating times without cleaning are less than 6–8 h until now. The addition of seeding crystals can have a positive effect on the stability of the MDC process. The vapor flow decreased during the experiment by only 9% with the gypsum seeding crystals and by 29% without seeding. When more than 5 g L^{-1} seeding crystals are added, the seeding, however, harms scaling (Yan *et al.* 2021).

In this study, a novel MDC process with seed crystallization technology and a newly introduced classifier for treating hypersaline solutions were developed and experimentally investigated. The work investigates the potential of long-term stability, high water recovery, and salt recovery without decreasing permeate quality from synthetic hypersaline solutions and the possibility of concentrating real wastewater in a long-term experiment.

METHODS AND MATERIALS

Mini NZLDMC plant

The design of a mini near-zero liquid discharge membrane crystallization (NZLDMC) plant consists of several key components. The main body of the plant comprises the membrane module, the classifier, and the heat exchanger module (Figure 1). These modules are specifically designed to account for hydrodynamic phenomena. The diameter of the classifier plays a critical role, as it directly influences the size of the crystals produced. Finally, the design also addresses the selection of materials for constructing the mini NZLDMC unit.

The used membrane is a polypropylene (PP) tubular membrane. The hydrophobic membrane is made from 3M® Accurel PP V8/2 HF. The mini-plant has an effective surface area of 0.017 m^2, a nominal pore size radius of 0.2 μm, a thickness of 1,550 μm, and a porosity of 73%. The inner and outer diameters of the membrane are 5.5 and 8.6 mm, respectively. The membrane selection is based on hydrophobicity and previous experiments using MD (Rezaei *et al.* 2018, 2020). The tubular membrane provides, in general, a better hydrodynamic condition compared to the flat sheet membrane and is generally regarded as providing less fouling. The heat exchanger section has a polypropylene graphite (PP-GR) tube with a length of 1 m and a surface area of 0.024 m^2, as well as a sedimentation section (Figure 1).

The feed is heated to a constant temperature in a co-current heat exchanger using a thermostat (Haake, NB 22) and then pumped into the lumen side of the tubular membrane at the top of the module. A magnetic flowmeter (Kobold, MIK 5N15AL343) indicates the flow rate, which is controlled by the speed of the peristaltic pump (Ismatec ISM 1080, Ecoline). The cold medium flows co-currently in the module at a temperature of 20 °C. The condensed permeate is collected in the permeate vessel and weighed by a balance (Kern, DE60K2N). The inlet and outlet temperatures of the membrane module, the permeate temperature in the permeate vessel, and the heat exchanger temperatures are measured with resistance thermometers (Kobold, MWE PT100). Conductivity meters are used to measure the electrical conductivity of the concentration loop (Kobold, LCI SG40MPF) and the permeate conductivity (Kobold, ACS-Z2T1G). An inline pH meter

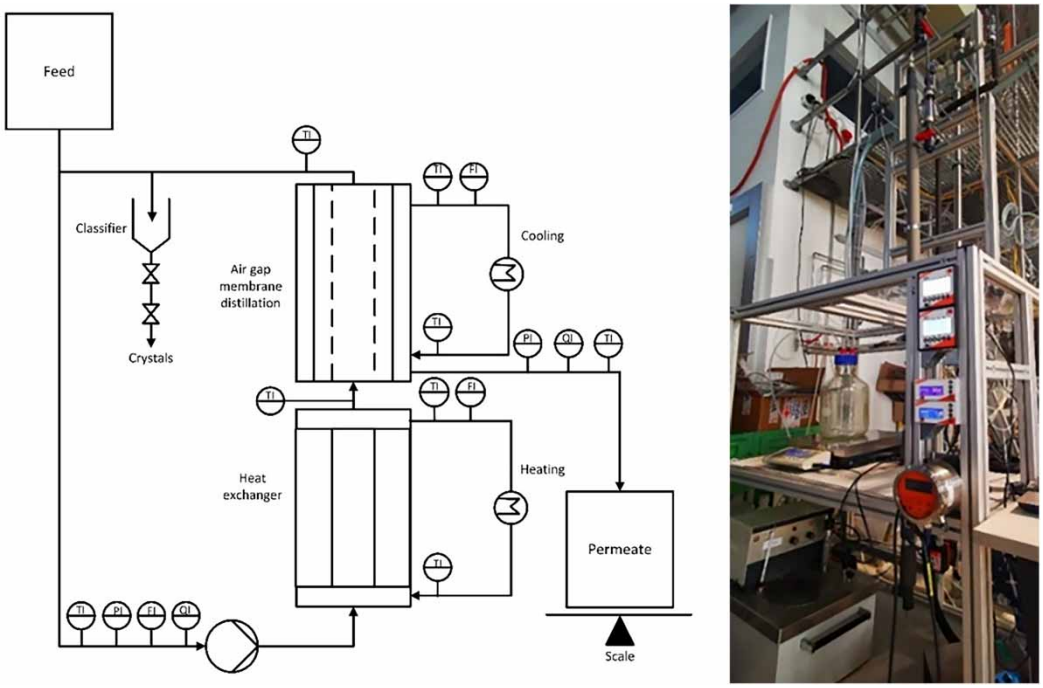

Figure 1 | Schematic drawing of the mini NZLDMC plant (left) and the plant (right).

(Kobold, gel-filled pH electrode) is used to measure the pH of the concentrating loop. The process conditions are adjusted so that the temperature of the loop in the membrane module remains constant to ensure continuous crystallization. The loop flow rate is 70–100 L h^{-1}, which was selected to prevent the crystals from growing in the mini-plant and blocking the pipelines. After the flow becomes constant, the permeate flux is calculated. The process is conducted continuously in a fed-batch experiment.

Design of the membrane and heat exchanger modules

To study the fluid dynamics within the membrane module and heat exchanger module, key parameters such as Reynolds number (Re), Prandtl number (Pr), Nusselt number (Nu), and heat transfer coefficient were considered. The Re plays a crucial role in mass transfer, concentration polarization coefficient (CPC), and temperature polarization coefficient (TPC). It distinguishes between laminar and turbulent flow regimes. As the Re number increases, flow transitions from laminar to turbulent occur, resulting in higher mass transfer coefficients and lower TPC and CPC due to enhanced turbulence within the boundary layers (Yu *et al.* 2021; Zhang *et al.* 2022). Furthermore, the concentration polarization at the surface influences the scaling depending on the Re number (Suga *et al.* 2022). The Re number is calculated based on

$$\mathrm{Re} = \frac{\rho v d}{\eta}, \tag{1}$$

where ρ (kg m^{-3}) is the density of the fluid, v (m s^{-1}) is the linear velocity of the fluid, d (m) is the hydraulic diameter of the flow pass, η (Pa s) is the viscosity of the fluid, and L is the length of the pipe, respectively. The Pr is defined as

$$\mathrm{Pr} = \frac{\eta}{\lambda}\mathrm{cp}, \tag{2}$$

where λ is thermal conductivity (W m^{-1} K^{-1}) and cp is the specific heat capacity of the hot feed (kJ kg^{-1} K^{-1}). The Nu for short pipes is given as a function of Re and Pr. Nu can be calculated for laminar flow ($\mathrm{Re} < 2{,}300$) and turbulent flow ($\mathrm{Re} > 2{,}300$). In the remaining laminar flow, the velocity must not exceed 0.234 m s^{-1} for a membrane diameter of

0.008 m (VDI 2006)

$$\mathrm{Nu}_{\mathrm{laminar}} = 0.664 \times \left(\mathrm{Re}\frac{d_i}{l}\right)^{1/2} \times \mathrm{Pr}^{1/3}. \tag{3}$$

As soon as the velocity is higher, turbulent flow occurs, which is (VDI 2006)

$$\mathrm{Nu}_{\mathrm{turbulent}} = A \times \frac{(\mathrm{Pr} \times \mathrm{Re})}{\left(1 + 12.7 \times \sqrt{A} \times \left(\mathrm{Pr}^{\left(\frac{2}{3}\right)} - 1\right)\right)} \times \left(1 + \left(\frac{d}{L}\right)^{\frac{2}{3}}\right), \tag{4}$$

where A is the coefficient, d is the membrane or heat exchanger diameter (m), and L is the length of the modules (m). The heat transfer coefficient was used to calculate the heat exchanger efficiency.

The heat transfer coefficient α for the heat exchanger efficiency can be calculated using

$$\alpha = \frac{\lambda}{d_o}\mathrm{Nu}, \tag{5}$$

$$k = \frac{1}{\left(\frac{d_o}{(d_i \cdot \alpha_i)} + \frac{d_o}{(2 \cdot \lambda)} \cdot \ln\left(\frac{d_o}{d_i}\right) + \frac{1}{\alpha_o}\right)}, \tag{6}$$

where d_o is the outer shell diameter (m), d_i is the inner shell diameter (m), α_o is the tube side heat transfer coefficient, and α_i is the shell side heat transfer coefficient (W m^{-2} K^{-1}). The main body, which consists of the membrane module and the heat exchanger module, was based on the previously mentioned and calculated parameters (Table 1). The lowest flow rate of 70 L h^{-1} gives an Re number of 7,400 for the membrane module, which is in the turbulent range. The Re number of the heat exchanger is 4,950 at a flow rate of 200 L h^{-1}, Pr is 2.90, and Nu is 36.93. Finally, the overall heat transfer coefficient k results in a value of 783 W m^{-2} K^{-1}. As the flow rate increases, the likelihood of fouling on the material decreases and the heat transfer coefficient on the feed side improves (Warsinger *et al.* 2015).

Performance of the MDC process

The permeate flux, water recovery, and salt rejection can evaluate the performance and effectiveness of the membrane process in water treatment.

The permeate flux is determined by the mass of the permeate at a given time, according to

$$J = \frac{\Delta m}{A \cdot \Delta t}, \tag{7}$$

Table 1 | Parameters for the design of the membrane module and the heat exchanger module

Properties		Membrane module	Heat exchanger module
n	Amount	1	1
A_{eff} (m^2)	Effective area	0.017	0.024
L (m)	Module length	1	1
V (mL)	Volume	24	45
D_{in} (m)	Diameter	0.0055	0.008
Re number (70 L h^{-1})	Reynolds number	7,400	5,430
k (W m^{-2} K^{-1})	Overall heat transfer coefficient	–	783

where J is the permeate flux (kg m^{-2} h^{-1}), Δm is the mass of collected permeate (kg), during the time (h) Δt, and A is the effective membrane area (m^2).

The mass flux J_m of solvent vapors in the MD process follows the dusty gas model (Lawson & Lloyd 1997) and is determined by the difference in water vapor pressure between the feed and the permeate.

$$J_m = K_m(P_{\mathrm{mf},i} - P_{\mathrm{mp},i}) = K_m \cdot \Delta P_{m,i}, \tag{8}$$

where K_m is the empirical mass transfer coefficient as a function of the temperature, pressure, and membrane structure. $\Delta P_{m,i}$ (Pa) is the water vapor pressure difference at the feed ($P_{\mathrm{mf},i}$) and the permeate side ($P_{\mathrm{mp},i}$). $P_{\mathrm{mf},i}$ and $P_{\mathrm{mp},i}$ values can be calculated from the Antoine equation, while the feed temperature has a direct influence.

$$P_{m,i} = \exp\left(A - \frac{B}{C + T_m}\right) \tag{9}$$

where T_m is feed temperature (K), The constants A, B, and C vary for different substances. Specifically for water, $A = 23.19$, $B = 3816.44$, and $C = -46.13$.

The water recovery in general is determined as

$$R_{\mathrm{batch}} = \frac{m_g}{m_p} \times 100, \tag{10}$$

where m_g is the mass of water and dissolved salt (kg) prepared as feed solution, hence the total mass, and m_p is the mass of the permeate (kg). Since the plant is initially filled with the feed, for the calculation of water recovery in an assumed continuous process, the dead volume of the plant is subtracted from the total mass to obtain the processed mass. The recovery is, therefore,

$$R_{\mathrm{con}} = \frac{m_g - m_{\mathrm{dead}}}{m_p} \cdot 100, \tag{11}$$

where m_{dead} is the mass of the dead volume in the plant (kg).

Influence of the temperature on the process

Particle sedimentation and separation

In the MDC process, crystallization has a significant influence on the quality and feasibility of the process, where controlling the size and growth of crystals is essential to prevent pipe blockages. The selection of the appropriate operating parameters is essential to avoid crystal deposits and enable the long-term operation of the process to obtain high water and salt recovery rates. The driving force of crystal growth is the supersaturation. The flow behavior in the settling tube changes the crystal size, which can be sediments. The size of the sinking crystals increases with a decrease in the settling tube diameter and with a decrease in temperature. The minimum separable particle diameter d is calculated using Stokes' law.

$$d = \sqrt{\frac{w \times 18\ \eta}{\Delta\rho \times g}}, \tag{12}$$

where w is the velocity of the liquid in the sedimentation tube (m s^{-1}), η is the viscosity of the liquid (kg m^{-1} s^{-1}), $\Delta\rho$ is the density difference between the seeding particle and the density of the solution (kg m^{-3}), and g is the gravity (m s^{-2}). The calculations of minimum separable particle diameter d are done for the mono-salt experiment with $\rho_s = 2,100$ kg m^{-3} (Figure 2, continuous line) and the wastewater experiment $\rho_s = 3,000$ kg m^{-3} (Figure 2, dotted line).

The velocity in the tube slows down by a factor of 10 from 0.34 to 0.034 m s^{-1} when the tube diameter is increased from 12 to 32 mm at a feed flow of 78 L h^{-1}. In the specific temperature range, the NaCl crystals settle earlier and only grow to 260 μm before the sediment due to the reduced velocity in the 32 mm settling tube (Figure 1, continuous line). By keeping the feed flow at 78 L h^{-1}, at a settling tube diameter of 12 mm, the crystals grow to 879 μm before they are separated by settling due to

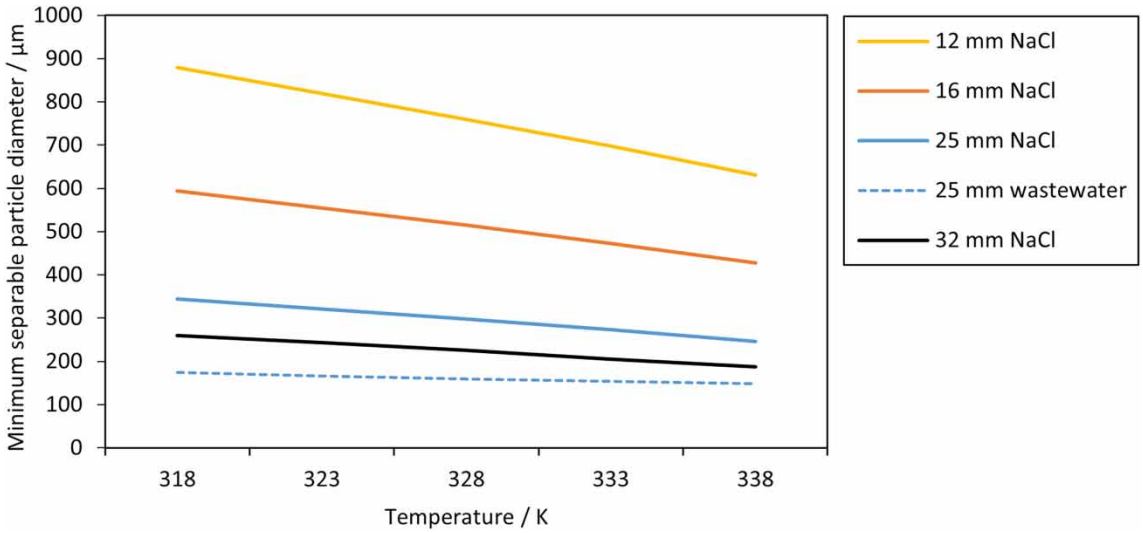

Figure 2 | Impact of the minimum separable particle diameter of particles with $\rho_S = 2,100$ kg m^{-3} and the temperature on the particle size. The dotted line shows the minimum separable particle diameter of the particle with $\rho_S = 3,000$ kg m^{-3}, corresponding to the crystals from wastewater.

a higher flow velocity. Calculations show that temperature affects crystal size, with crystals being 25–40% smaller at 338 compared to 318 K.

The ability to control crystal growth via the settling tube allows the process to be adapted directly to the size of the salt that is required. With the given tube diameters and given feed velocity, the separated crystal size range is from 829 to 205 μm for a 22.5% NaCl solution.

The tube velocity for the wastewater experiment was 0.046 m s^{-1}with the 25 mm tube diameter. The crystals based on the theory should begin to settle with a diameter of 174 μm at 318 K and 148 μm at 338 K (Figure 1, dotted line).

Salt recovery

After crystallization is complete, the settled crystals are removed from the classifier. These crystals are then subjected to a filtration process. After filtration, the crystals are weighed to determine their mass. The mass of the crystals obtained is used to calculate the salt recovery.

$$S_{\text{rec}} = \frac{m_{\text{cry}}}{m_{\text{tot}}} \times 100, \tag{13}$$

where m_{cry} is the mass of the recovered salt from the process (kg) and m_{tot} is the total mass of the salt in the feed solution (kg).

Crystal characterization

The precipitated crystals were observed with an optical microscope (Keyence VHX-7000), which provides exceptional depth of field for flexible crystal viewing, and the crystal sizes (2D) were characterized with the microscope software and Image J 1.54h software.

MATERIAL

Several factors were considered in the selection of materials, including corrosion resistance, weight, and the ability to expand the modules easily. Metals such as iron are susceptible to corrosion problems because most wastewater contains chlorides. These materials will rust through in a brief period and will not be used for extended periods. In addition, metals tend to be heavier and more expensive than plastics. Alloys, which are considered for the process because they are more resistant to salts, are even more expensive. The temperature range and maximum temperature at which a metal can be used are much higher than for plastic. The maximum temperature for a short time at which unplasticized polyvinyl chloride (PVC-U) piping can be used is approximately 70 °C. The driving force of MD is the vapor pressure difference. Hence, the boiling

point of the solution does not need to be reached. An advantage is that the feed solution can be heated by solar energy. The energy consumption of this process can be covered by renewable energy. A major advantage of plastic is that it is inexpensive. Investment costs for plastic equipment are lower than for metallic materials. For the material of the condenser plate, copper was chosen so that the water vapor could condense on the cooled surface of the air gap. These were among the reasons for the choice of materials for the plant (Table 2).

Feed solutions

Properties of the synthetic solutions

Different feed solutions were prepared (Table 3). For experiment 1, a 1.2 L mono-salt solution with NaCl (Roth, >99%) and 0.05 wt% of silica sand was prepared. Considering the concentration, a higher concentration than the one that typically results from desalination brine solution was selected to be closer to the crystallization point and to speed up the initial phase. The NaCl solution was concentrated above the solubility limit until the salt began to crystallize and the crystals settled down in the collector tube. For experiment 2, a 1 L multi-salt solution containing NaCl, $CaCl_2 \cdot 6H_2O$ (Acros Organics, 98 + %), and 0.05 wt% of silica sand is used. These applied salts are commonly found in wastewater samples from desalination.

For the multi-salt fractional crystallization experiment, a large gap was chosen between solubilities in water so that they do not precipitate simultaneously or shortly after each other by adjusting the temperature. The feed temperature was optimized by systematically screening a range of operating temperatures, ensuring optimal permeate flux and crystallization occurrence. $CaCl_2$ shows a temperature-dependent behavior; as the temperature increases, the solubility of the salts improves, which positively influences the permeate flux. When solubility increases, more solute particles are dissolved in the solvent, resulting in a higher concentration of solute in the solution. This higher concentration can create a greater concentration gradient across the membrane, which can drive a higher permeation rate. Specifically, at a temperature of 55 °C, the solubility of NaCl is 369 g L^{-1}, while that of $CaCl_2$ is significantly higher at 1,300 g L^{-1}.

Properties of the real wastewater

Highway wastewater of 26 L was taken from a storage tank in Upper Austria. The water was light green, with organic impurities. In the first step, the wastewater solution was filtered with filter paper (Schleicher and Schuell 598[3], diameter of 185 mm, mesh size of 2.2 μm). The highway wastewater components after filtration are shown in Table 4 and were determined by Inductively Coupled Plasma Optical Emission spectroscopy (ICP-OES) (Thermo Fisher, iCAP Pro).

Table 2 | Used material for the main body of the mini NZLDMC plant

Heat exchanger	**Tube in shell type**
Tube	PP-GR – thermally conductive (Technoform Germany)
Shell	Standard PVC-U pipe
Crystal separator	**Settling tube**
Tube	Standard PVC-U pipe
Collector	Transparent PVC-U pipe
Membrane module	**Tube in shell type**
Membrane tube	ACCUREL® PP V8/2HF 0.2 μm (3M Germany)
Condensator tube	Copper
Shell	Standard PVC-U pipe

Table 3 | Experiments and initial salt concentrations for experiment 1 (mono-salt) and experiment 2 (multi-salt)

	Experiment 1: Mono-salt	**Experiment 2: Multi-salt**
NaCl (g L^{-1})	290	255
$CaCl_2 \cdot 6\ H_2O$ (g L^{-1})	–	255

Table 4 | Water characteristics of the saline highway wastewater used as feed solution

	Experiment 3: highway wastewater
Conductivity (mS cm^{-1})	2
pH	7.9
Na (mg L^{-1})	3,540
K (mg L^{-1})	56
Mg (mg L^{-1})	60
Ca (mg L^{-1})	17
Tl (mg L^{-1})	5

The physical parameters of the water quality are summarized as follows. The conductivity of the highway wastewater was maintained at 2 mS cm^{-1}. The pH of the wastewater was slightly basic at 7.9. The main component of the wastewater is Na; it also contains K, Mg, Ca, and Tl.

Seeding crystals

The seed crystals prevent unwanted nucleation on the membrane surface and reduce the wetting behavior on the membrane surface (Yan *et al.* 2021). Commercially available SiO_2 was used as the seed crystal, as it hardly dissolves in water. The suggested amount of seed crystals should fall between 0.05 and 1 wt% to minimize contamination in the produced salt. At least 90% of the silica sand is between 0.21 and 0.3 mm in size.

RESULTS AND DISCUSSION

The design and construction of the NZLDMC mini-plant were successfully completed, considering all the specified details. Experiments were conducted at the NZLDMC mini-plant, focusing on three different types of investigations. In the first experiment, a mono-salt solution was used to investigate the performance of the mini-plant. Subsequently, a multi-salt solution was prepared to test the performance of the plant with multiple salts and to investigate the separation performance of the salts. Finally, real highway wastewater was used to achieve high water recovery, concentrate the solution, and evaluate the behavior of the wastewater on the membrane.

Mono-salt experiment

The NZLDMC experiments were conducted using a 290 g L^{-1} NaCl mono-salt solution. The feed solution was subsequently heated to 55 $\pm$ 1 °C. Throughout the experiment, the temperature was maintained at a constant level.

The permeate flux can be observed to increase with a higher feed flow (Figure 3). With an increase of 23% of the feed flow from 1,300 to 1,600 mL h^{-1}, the permeate flux increased from 2.5 to 2.9 kg m^{-2} h^{-1}, an increase of 16%. Both flows remained nearly constant over the operational time. Higher flow rates increase turbulences and improve mass and heat transfer in the system, resulting in higher permeate fluxes (Winter *et al.* 2011; Schwantes *et al.* 2018). The permeate conductivity is constant during the experiment and on average 0.7 µS cm^{-1}. The permeate conductivity did not increase over the experiment, which shows that no wetting occurred during the experiment. The retentate at the end of the experiment has a concentration of 330 g L^{-1}. The concentration observed is below the solubility limit of NaCl at 55 °C, which indicates the influence of concentration polarization. A water recovery R_{con} of 93% was achieved at the end of the experiment. The salt recovery was approximately 79% at the end of the experiments. The experiments with the mono-salt solution show promising results. Since the permeate flux was constant and the recovery of salt and water with the mono-salt was successful, a multi-salt solution was used in the next step.

Crystal size characterization

A key parameter in the characterization of solid particles is the crystal size distribution (CSD), and the crystal sizes determine the quality of the end product (Drioli *et al.* 2004). To determine the crystal sizes, the crystals were taken from the classifier's mini-plant, which had a diameter of 12 mm. The sizes were then analyzed with a Keyence microscope. Figure 4 depicts the size of the crystals from the process, with a minimum and a maximum size of 500 and 1,100 µm, The respective diameters are

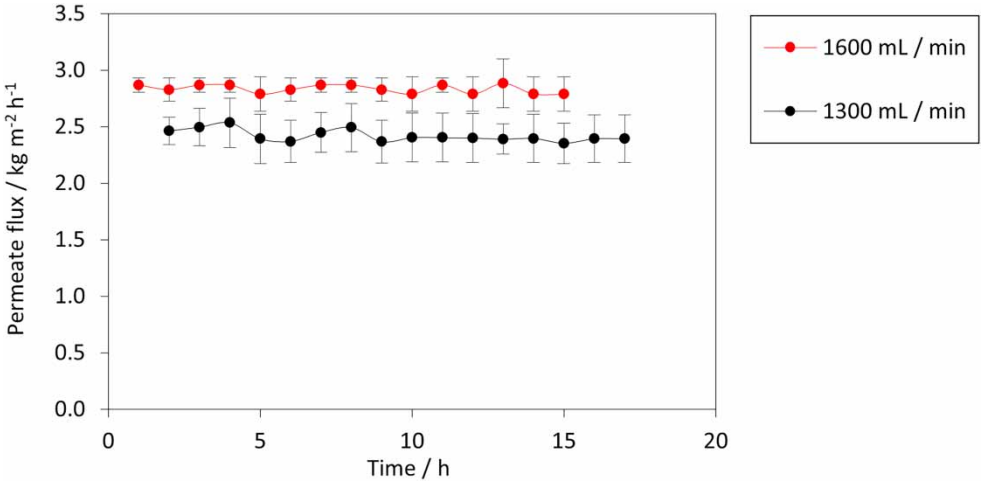

Figure 3 | Permeate flux ($T = 55 \pm 1$ °C) under different feed flow over the experiment time.

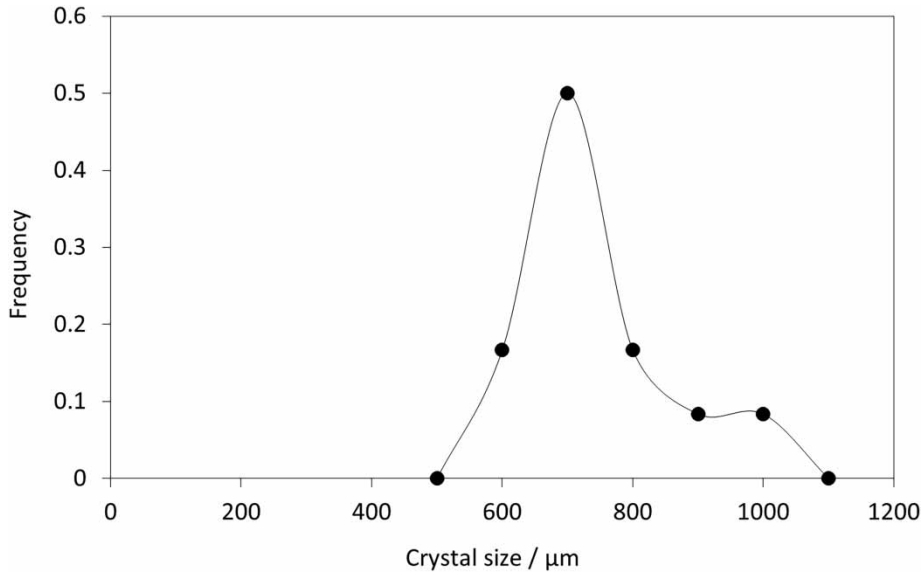

Figure 4 | The measured size distribution of NaCl crystals. The key sizes of the NaCl crystals are $d_{16} = 596$ µm, $d_{50} = 666$ µm, and $d_{84} = 808$ µm. CSD shows that the largest number of crystals is between 500 and 850 µm.

$d_{16} = 596$ µm, $d_{50} = 666$ µm, and $d_{84} = 808$ µm. The calculated minimum separable particle diameter is 14% higher than measured d_{50} and 6% lower than d_{84}, and, therefore, a reasonable agreement between experiment and theory is given. The differences in crystal sizes between calculated and measured sizes can be referred to be due to agglomeration, breakage, or additional crystal growth between obtaining the sample and measuring. These variables were not considered in the calculations.

Multi-salt experiment

The NZLDMC experiments were conducted using a multi-salt solution, which was prepared by mixing 255 g L^{-1} NaCl and 255 g L^{-1} $CaCl_2 \cdot 6\ H_2O$. The feed solution was subsequently heated to 55 ± 1 °C. Throughout the experiment, the temperature was maintained at a constant level. The resulting permeate flux increases from 1.53 to 1.76 kg m^{-2} h^{-1} and stays constant until the end of the experiment (Figure 5, black dots). Comparing the mono-salt and multi-salt experiments, the permeate flux

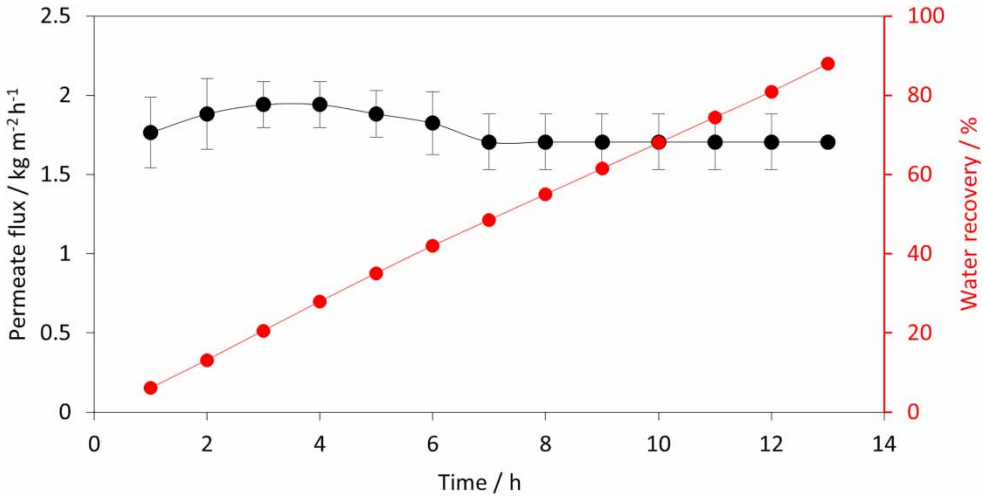

Figure 5 | The permeate flux (black dots) and the water recovery of the multi-salt solution experiment using of 255 g L^{-1} NaCl and 255 g $^{-1}$ CaCl2 · 6 H_2O at a temperature of $T = 55 \pm 1$ °C.

of the multi-salt experiment is lower than that of the mono-salt solution. This can be referred to a higher salt content and the resulting lower vapor pressure (El-Bourawi *et al.* 2006; Alkhudhiri & Hilal 2017).

The multi-salt solution experiment results in an R_{con} of 89% (Figure 5, red dots). A salt recovery of 60% in total is achieved without compromising the quantity and quality of the permeate. The permeate conductivity is on average 1.5 μS cm^{-1}.

Crystal characterization

After the crystal fractions were removed from the classifier, they were examined more closely under the microscope. As can be seen in Figure 6 (left and right), the crystal morphology of the two fractions was clearly different. The figure on the left shows cubic crystals of different sizes, which is very typical for NaCl crystals. The figure on the right shows unstructured grown crystals of $CaCl_2$.

Highway wastewater

In the final phase, highway wastewater was concentrated and treated to demonstrate the feasibility of the process with real wastewater. During the experiment, the temperature was changed four times to observe the permeate flux at different temperatures (Table 5) (El-Bourawi *et al.* 2006).

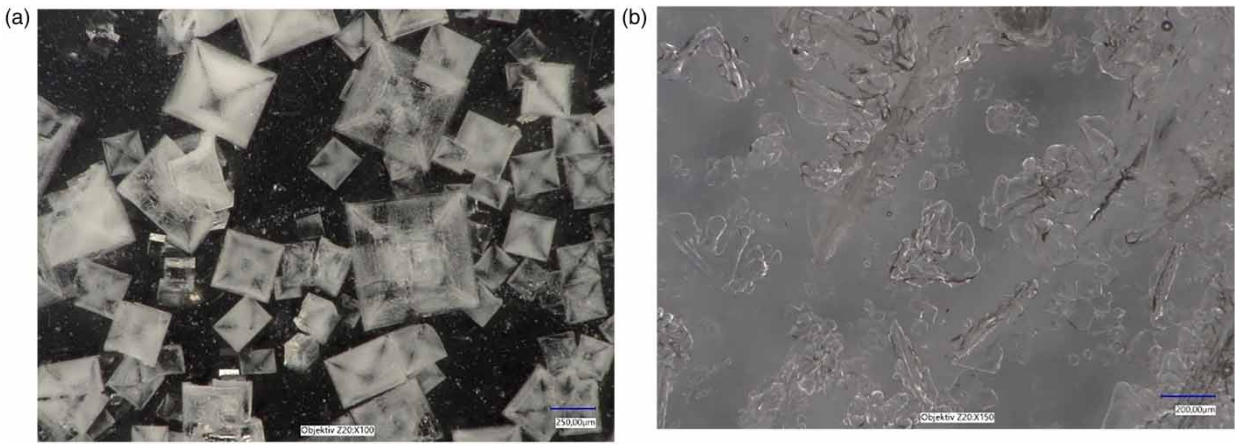

Figure 6 | First fraction of salt: cubic NaCl-like crystal in different sizes (left) and second fraction: colorless and unstructured grown crystals $CaCl_2$ (right).

Table 5 | Operating temperature of the highway wastewater during the experiment and the permeate fluxes of the MDC process

Day	Temperature (°C)	Permeate flux (kg m^{-2} h^{-1})
1–4	61	1.1
5–8	67	2.3
9–19	70	4.1
19–22	65	2.4

Between days 1 and 4 of the experiment, the temperature was set to 61 °C, while the permeate flux was 1.1 kg m^{-2} h^{-1}. The temperature was increased to 67 °C on the fifth day, resulting in an average increase in permeate flux of 2.3 kg $^{-2}$ h^{-1}. The temperature was raised again to 70 °C on the ninth day. Between the 9th and 12th days, the permeate flux remained steady at 4.1 kg m^{-2} h^{-1}. On the 14th day, it peaked at a maximum of 4.7 kg m^{-2} h^{-1} and then decreased to 3.9 kg m^{-2} h^{-1}. The maximum peak can be caused by a partial wetting of some pores (Rezaei *et al.* 2018). From day 18 onward, the permeate flux remained constant. Subsequently, the temperature was reduced to 65 °C, and the permeate flux decreased to 2.3 kg m^{-2} h^{-1} and further to 1.9 kg m^{-2} h^{-1} on day 22. The findings indicate that an increase in the feed temperature shows an increase in the permeate flux, resulting from a change in the driving force for mass transfer. This can be explained by the Antoine equation: by increasing the temperature, the vapor pressure increases exponentially (Edwie & Chung 2012; Qu *et al.* 2021). The experiment was concluded on day 22 due to the absence of further highway wastewater. The water recovery showed a linear increase during the experiment, reaching 99% (Figure 7).

At the start of the experiment, the wastewater exhibited low salinity, with a conductivity of 2 mS cm^{-1}. After 22 days, the salinity increased and reached a conductivity of 13 mS cm^{-1}. During the experiment, it was possible to recover 3 g of a hardly soluble salt mixture. The permeate conductivity of the experiment was on average 25 µS cm^{-1}.

Crystal size characterization of the real wastewater

The crystals were taken from the classifier's mini-plant, which had a diameter of 25 mm, to determine the crystal size. In the next step, the crystals were filtered and dried. The calculated crystal size is between 100 and 400 µm. Figure 8 depicts the crystal size from the process with a minimum and a maximum size of 0 and 400 µm and shows a $d_{16} = 42$ µm, a $d_{50} =$ 95 µm, and a $d_{84} = 178$ µm. In comparison between the 25 and the 12 mm of the settling tube diameter, the crystals are 5.5 times smaller. The calculated minimum separable particle diameter is 55% higher than the measured d_{50} and 17% lower than the measured d_{84}. Crystals may have precipitated after filtration and led to a change in the CSD. The offline measurement of crystal sizes is not optimal for these experiments as agglomeration, breaking, and recrystallization can lead to larger deviations. Therefore, an online measurement will be installed in the future.

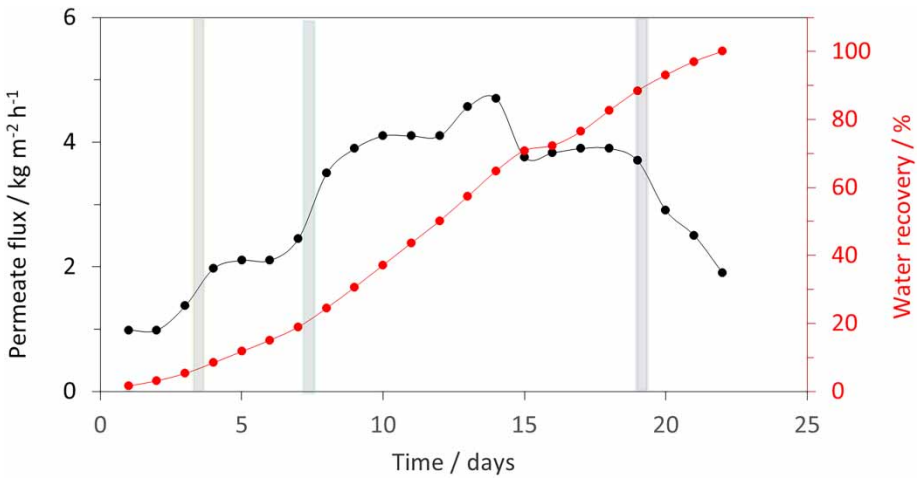

Figure 7 | Permeate flux and water recovery of the real highway wastewater with varying temperature over 22 days.

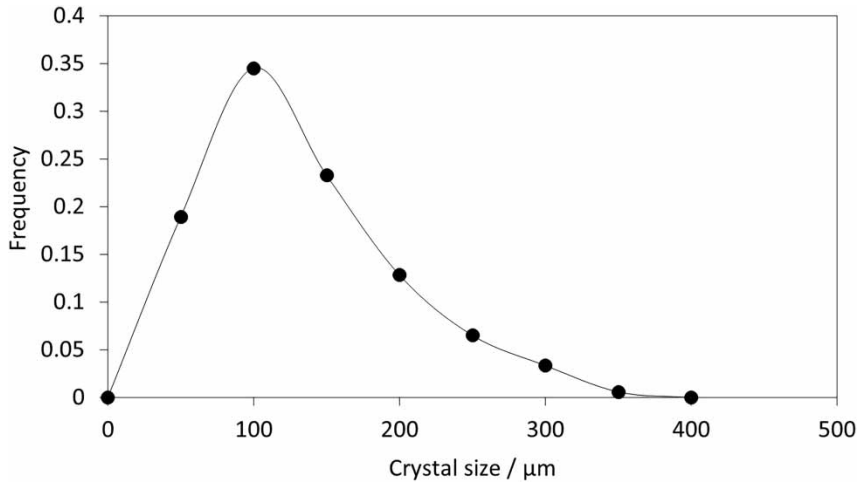

Figure 8 | The size distribution of the NaCl crystals is between 0 and 400 μm for the wastewater experiment. The key crystal sizes are $d_{16} = 42$ μm, $d_{50} = 95$ μm, and $d_{84} = 178$ μm.

CONCLUSIONS

The study demonstrated the feasibility and advantages of using seeded near-ZLD membrane crystallization as an alternative to conventional brine evaporation and crystallization processes; due to the needed temperature in the process, it is possible to use solar energy to heat the feed solution. The investigation successfully utilized seeding processes in the NZLDMC to concentrate synthetic mono- and multi-salt solutions. Long-term stability over 18 days of permeate flux could be achieved by implementing a classifier and avoiding the settling of crystals on the membrane. The effect of salt crystals and seeds on membrane performance was investigated under various operating conditions. For the mono-salt experiment, a recovery of 93% was achieved. The multi-salt experiment revealed that crystallization fractionation is possible and during these experiments, a recovery of 89% was achieved. For the real wastewater experiment coming from highway water, a recovery of even 99% could be monitored. A longer-term stability of the membrane could be achieved by the seeding crystallization. These results demonstrate the potential of NZLDMC for continuous operation and efficient water reclamation by increasing, in addition, the operational time further compared to the existing literature.

Future research endeavors will delve deeper into the effects of different salts, salt concentrations, seeding concentrations, and process parameters for mono-salt solutions, multi-salt solutions, and wastewater treatment. The objective is to achieve a consistent permeate flux over long-term experiments without compromising the quantity or quality of the permeate. This will involve optimizing operational parameters and exploring different seeding concentrations, for example, cooperation with renewable energy sources, particularly solar energy, to reach sustainability goals. Subsequently, the aim is to scale up the mini NZLDMC plant to a pilot plant, incorporating multiple membranes and heat exchangers within the membrane module and heat exchanger module, respectively. This scale-up process will facilitate the integration and optimization of seeding crystallization and MD processes, paving the way for their application in various industrial processes and municipal wastewater treatment.

Overall, this study provides valuable insights into the integration of seeding crystallization and MD processes, serving as a guide for scaling up and implementing this promising technology in practical applications.

DATA AVAILABILITY STATEMENT

All relevant data are included in the paper or its Supplementary Information.

CONFLICT OF INTEREST

The authors declare there is no conflict.

REFERENCES

Ahmad, N. & Baddour, R. E. 2014 A review of sources, effects, disposal methods, and regulations of brine into marine environments. *Ocean & Coastal Management* **87**, 1–7.

Al-Agha, M. R. & Mortaja, R. S. 2005 Desalination in the Gaza Strip: Drinking water supply and environmental impact. *Desalination* **173**, 157–171.

Alkhudhiri, A. & Hilal, N. 2017 Air gap membrane distillation: A detailed study of high saline solution. *Desalination* **403**, 179–186.

Almasri, D., Mahmoud, K. A. & Abdel-Wahab, A. 2015 Two-stage sulfate removal from reject brine in inland desalination with zero-liquid discharge. *Desalination* **362**, 52–58.

Bello, A. S., Zouari, N., Da'ana, D. A., Hahladakis, J. N. & Al-Ghouti, M. A. 2021 An overview of brine management: Emerging desalination technologies, life cycle assessment, and metal recovery methodologies. *Journal of Environmental Management* **288**, 112358.

Chen, G., Lu, Y., Krantz, W. B., Wang, R. & Fane, A. G. 2014 Optimization of operating conditions for a continuous membrane distillation crystallization process with zero salty water discharge. *Journal of Membrane Science* **450**, 1–11.

Conidi, C., Macedonio, F., Ali, A., Cassano, A., Criscuoli, A., Argurio, P. & Drioli, E. 2018 Treatment of flue gas desulfurization wastewater by an integrated membrane-based process for approaching zero liquid discharge. *Membranes* **8**, 1–12.

Creusen, R., van Medevoort, J., Roelands, M., van Renesse Duivenbode, A., Hanemaaijer, J. H. & van Leerdam, R. 2013 Integrated membrane distillation–crystallization: Process design and cost estimations for seawater treatment and fluxes of single salt solutions. *Desalination* **323**, 8–16.

Damtie, M. M., Hailemariam, R. H., Woo, Y. C., Park, K.-D. & Choi, J.-S. 2019 Membrane-based technologies for zero liquid discharge and fluoride removal from industrial wastewater. *Chemosphere* **236**, 124288.

Date, M., Patyal, V., Jaspal, D., Malviya, A. & Khare, K. 2022 Zero liquid discharge technology for recovery, reuse, and reclamation of wastewater: A critical review. *Journal of Water Process Engineering* **49**, 103129.

Dehghani, S., Massah Bavani, A. R., Roozbahani, A., Gohari, A. & Berndtsson, R. 2022 Towards an integrated system modeling of water scarcity with projected changes in climate and socioeconomic conditions. *Sustainable Production and Consumption* **33**, 543–556.

Drioli, E., Curcio, E., Criscuoli, A. & Di Profio, G. 2004 Integrated system for recovery of $CaCO_3$, NaCl and $MgSO_4{\cdot}7H_2O$ from nanofiltration retentate. *Journal of Membrane Science* **239**, 27–38.

Drioli, E., Di Profio, G. & Curcio, E. 2012 Progress in membrane crystallization. *Current Opinion in Chemical Engineering* **1**, 178–182.

Edwie, F. & Chung, T.-S. 2012 Development of hollow fiber membranes for water and salt recovery from highly concentrated brine via direct contact membrane distillation and crystallization. *Journal of Membrane Science* **421–422**, 111–123.

El-Bourawi, M. S., Ding, Z., Ma, R. & Khayet, M. 2006 A framework for better understanding membrane distillation separation process. *Journal of Membrane Science* **285**, 4–29.

Gilron, J., Folkman, Y., Savliev, R., Waisman, M. & Kedem, O. 2003 WAIV – Wind aided intensified evaporation for reduction of desalination brine volume. *Desalination* **158**, 205–214.

Guan, G., Wang, R., Wicaksana, F., Yang, X. & Fane, A. G. 2012 Analysis of membrane distillation crystallization system for high salinity brine treatment with zero discharge using aspen flowsheet simulation. *Industrial & Engineering Chemistry Research* **51**, 13405–13413.

Gustafson, R. D., Hiibel, S. R. & Childress, A. E. 2018 Membrane distillation driven by intermittent and variable-temperature waste heat: System arrangements for water production and heat storage. *Desalination* **448**, 49–59.

Hristov, J., Barreiro-Hurle, J., Salputra, G., Blanco, M. & Witzke, P. 2021 Reuse of treated water in European agriculture: Potential to address water scarcity under climate change. *Agricultural Water Management* **251**, 106872.

Jones, E., Qadir, M., van Vliet, M. T. H., Smakhtin, V. & Kang, S.-M. 2019 The state of desalination and brine production: A global outlook. *The Science of the Total Environment* **657**, 1343–1356.

Julian, H., Nurgirisia, N., Sutrisna, P. D. & Wenten, I. G. 2022 Advances in seawater membrane distillation (SWMD) towards stand-alone zero liquid discharge (ZLD) desalination. *Reviews in Chemical Engineering* **38**, 959–990.

Lawson, K. W. & Lloyd, D. R. 1997 Membrane distillation. *Journal of Membrane Science* **124**, 1–25.

Mekonnen, M. M. & Hoekstra, A. Y. 2016 Four billion people facing severe water scarcity. *Science Advances* **2**, e1500323.

Morillo, J., Usero, J., Rosado, D., El Bakouri, H., Riaza, A. & Bernaola, F.-J. 2014 Comparative study of brine management technologies for desalination plants. *Desalination* **336**, 32–49.

Panagopoulos, A. 2021 Beneficiation of saline effluents from seawater desalination plants: Fostering the zero liquid discharge (ZLD) approach – A techno-economic evaluation. *Journal of Environmental Chemical Engineering* **9**, 105338.

Panagopoulos, A., Haralambous, K.-J. & Loizidou, M. 2019 Desalination brine disposal methods and treatment technologies – A review. *The Science of the Total Environment* **693**, 133545.

Peters, C. D. & Hankins, N. P. 2021 Making zero-liquid discharge desalination greener: Utilising low-grade heat and vacuum membrane distillation for the regeneration of volatile draw solutes. *Desalination* **507**, 115034.

Qu, M., You, S. & Wang, L. 2021 Insights into nucleation and growth kinetics in seeded vacuum membrane distillation crystallization. *Journal of Membrane Science* **620**, 118813.

Raff, Z. & Earnhart, D. 2018 Effect of cooperative enforcement strategies on wastewater management. *Economic Inquiry* **56**, 1357–1379.

Rao, G., Hiibel, S. R. & Childress, A. E. 2014 Simplified flux prediction in direct-contact membrane distillation using a membrane structural parameter. *Desalination* **351**, 151–162.

Rezaei, M., Warsinger, D. M., Lienhard V, J. H., Duke, M. C., Matsuura, T. & Samhaber, W. M. 2018 Wetting phenomena in membrane distillation: Mechanisms, reversal, and prevention. *Water Research* **139**, 329–352.

Rezaei, M., Alsaati, A., Warsinger, D. M., Hell, F. & Samhaber, W. M. 2020 Long-running comparison of feed-water scaling in membrane distillation. *Membranes* **10**, 1–21.

Schwantes, R., Bauer, L., Chavan, K., Dücker, D., Felsmann, C. & Pfafferott, J. 2018 Air gap membrane distillation for hypersaline brine concentration: Operational analysis of a full-scale module – New strategies for wetting mitigation. *Desalination* **444**, 13–25.

Shah, K. M., Billinge, I. H., Chen, X., Fan, H., Huang, Y., Winton, R. K. & Yip, N. Y. 2022 Drivers, challenges, and emerging technologies for desalination of high-salinity brines: A critical review. *Desalination* **538**, 115827.

Shomar, B. & Hawari, J. 2017 Desalinated drinking water in the GCC countries – The need to address consumer perceptions. *Environmental Research* **158**, 203–211.

Suga, Y., Takagi, R. & Matsuyama, H. 2022 Effect of hollow fiber membrane properties and operating conditions on preventing scale precipitation in seawater desalination with vacuum membrane distillation. *Desalination* **527**, 115578.

Tun, C. M., Fane, A. G., Matheickal, J. T. & Sheikholeslami, R. 2005 Membrane distillation crystallization of concentrated salts – Flux and crystal formation. *Journal of Membrane Science* **257**, 144–155.

VDI-Wärmeatlas 2006 *VDI-Wärmeatlas*, 10th edn. (in German), Springer, Berlin.

Warsinger, D. M., Swaminathan, J., Guillen-Burrieza, E., Arafat, H. A. & Lienhard V, J. H. 2015 Scaling and fouling in membrane distillation for desalination applications: A review. *Desalination* **356**, 294–313.

Winter, D., Koschikowski, J. & Wieghaus, M. 2011 Desalination using membrane distillation: Experimental studies on full scale spiral wound modules. *Journal of Membrane Science* **375**, 104–112.

Yan, Z., Lu, Z., Chen, X., Fan, G., Qu, F., Pang, H. & Liang, H. 2021 Integration of seeding- and heating-induced crystallization with membrane distillation for membrane gypsum scaling and wetting control. *Desalination* **511**, 115115.

Yu, Z., Wang, X., Li, W. & Chen, S. 2021 Computational fluid dynamics modeling of hollow membrane filtration for concentration polarization. *Water* **13**, 3605.

Zhang, T., Laborie, S. & Cabassud, C. 2022 Optical method for in operando study of membrane distillation wetting: Development for desalination and potential for exploring wetting dynamics. *Desalination* **539**, 115944.

Zhao, S., Hu, S., Zhang, X., Song, L., Wang, Y., Tan, M., Kong, L. & Zhang, Y. 2020 Integrated membrane system without adding chemicals for produced water desalination towards zero liquid discharge. *Desalination* **496**, 114693.

First received 21 July 2023; accepted in revised form 31 January 2024. Available online 17 February 2024